Hindawi
Mathematical Problems in Engineering
Volume 2020, Article ID 7312521, 14 pages
https://doi.org/10.1155/2020/7312521

Research Article

A Continuous-Discrete Finite Memory Observer Design for a Class of Nonlinear Systems: Application to Fault Diagnosis

Tingting Zhang, Frédéric Kratz, Yunhui Hou, and Vincent Idasiak

INSA Centre Val-de-Loire, Bourges 18022, France

Correspondence should be addressed to Tingting Zhang; tingting.zhang@insa-cvl.fr

Received 9 March 2020; Revised 22 May 2020; Accepted 4 June 2020; Published 16 July 2020

Academic Editor: Jerzy Baranowski

This paper aims to develop a continuous-discrete finite memory observer (CD-FMO) for a class of nonlinear dynamical systems modeled by ordinary differential equations (ODEs) with discrete measurements. The nonlinear systems under consideration are at least *locally* Lipschitz, which guarantees the existence and uniqueness of solution at each time instant. The proposed nonlinear observer uses a finite number of collected measurements to estimate the system state in the presence of measurement noise. Besides, a one-step prediction algorithm incorporated with an iterative-update scheme is performed to solve the integral problem caused by system nonlinearity, and an analysis of the numerical integration approximation error is given. The properties of estimation performance have been further proved in deterministic case and been analyzed by Monte Carlo simulation in stochastic cases. It is worth noting that the presented method has a finite-time convergence, while most nonlinear observers are usually asymptotically convergent. Another advantage of CD-FMO is that it has no initial value problem. For the application purpose, residuals are generated to implement fault detection cooperated with Cumulative Sum (CUSUM) control charts, while a bank of CD-FMOs is adopted to realize fault isolation for different sensor and actuator faults of the considered nonlinear robotic arm. The robustness and effectiveness of the proposed approach are illustrated via the simulation results.

1. Introduction

Over past decades, it was noticed that state estimation, especially observer, plays an important role in the modern control theory and practice [1–3]. As the real engineering systems became more and more complex, the corresponding growing demand of observer design for complex nonlinear systems have gained increasing consideration. The pioneer works can be traced to [4, 5], which represents the major pseudo-linear techniques nowadays. However, in order to well ensure the existence of the coordinate transformation in these approaches, the established conditions are extremely difficult to satisfy in practice [6]. In the meantime, numerous system nonlinearities can be regarded as *globally* Lipschitz or at least *locally* [7]. Hence, there also exist several methods which focus on developing the observers directly based on the original nonlinear Lipschitz systems by solving linear matrix inequalities (LMIs) under certain assumptions or using the high gain observer [6–9]. As we knew that the dynamics of most engineering systems are naturally continuous [10], e.g., trajectories of vehicles and flow of electric current, it is more convenient and accurate to model the physical processes in continuous time with nonlinear differential equations. Meanwhile, observations are usually taken at discrete time instants when using digital sensors. For this reason, there is a significant amount of observer designs that has been investigated in the literature based on continuous-discrete modeling [3, 8, 11, 12].

Observer-based method has also been widely used in fault detection and isolation (FDI) of many fields such as PEM fuel cell and heat-exchanger/reactor system [13–15]. As examined in [16, 17], that model-based diagnosis method will be affected with divergence due to the accumulation of modeling uncertainties. Furthermore, state estimation based on infinite memory (i.e., all the process history) may result in the insensitivity to recent measurements which might have the

clues of a fault in incipient stage [18]. Thus, the corresponding researches like fading filter [19] and finite memory observer are naturally explored. Finite memory observer (FMO) was first proposed by Medvedev [20] for linear system in the deterministic framework, which indicates that this observer is extremely efficient for state estimation. Afterwards, the robustness and sensitivity of this approach were addressed by Nuninger and Graton [18, 21]. Kratz et al. have then synthesized this observer in fault diagnosis of linear system [22] and hybrid system [23]. All these previous researches reveal that finite memory observer provides a great potential in state estimation as well as in fault diagnosis.

Therefore, the main contribution of this paper is that we develop a nonlinear continuous-discrete finite memory observer (CD-FMO) for a class of nonlinear Lipschitz system. It has been proven that the designed observer has a finite-time convergence and good robustness against measurement noise. Moreover, we also perform a rapid fault detection and an accurate fault isolation to a single-link robotic arm by using the proposed nonlinear CD-FMO in the presence of measurement noise.

The work of this paper is organized as follows: Section 2 introduces the statements of problem with considered continuous-discrete nonlinear system. In Section 3, we present the construction of the proposed nonlinear CD-FMO together with an iterative-update algorithm for numerically approximating integration due to the nonlinearity of system. In addition, we also give a detailed demonstration of the finite-time convergence. The criteria of how to choose the window length is also stated in this section. In Section 4, we apply our approach to a nonlinear state-space model of a single-link robotic arm. A detailed analysis is provided with respect to selection of window length, estimation performance, numerical integration error analysis, and robustness analysis, respectively. In terms of application in fault diagnosis, different sensor faults and actuator fault, which are the two typical faults in actual physical system, have been illustrated in Section 5. Conclusions and the perspectives of future works are summarized in Section 6.

2. Problem Statement

We consider a class of continuous-discrete nonlinear systems described by the following state-space equation:

$$\dot{x}(t) = Ax(t) + Bu(t) + \Phi(x) + Gw(t), \tag{1a}$$

$$y(k) = Cx(k) + v(k), \tag{1b}$$

where $x \in \mathbb{R}^n$, $y \in \mathbb{R}^p$, and $u \in \mathbb{R}^q$ are continuous state vector, discrete measurement vector, and continuous input vector, respectively. T_s is the sampling period of measurement (i.e., $\exists k \in \mathbb{N} \mid t = k \times T_s$). $A \in \mathbb{R}^{n\times n}$, $B \in \mathbb{R}^{n\times q}$, $G \in \mathbb{R}^{n\times n}$, and $C \in \mathbb{R}^{p\times n}$ are known matrices. The nonlinearity $\Phi(x)$ is a nonlinear function with respect to state x. $\Phi(x)$ is at least *locally* Lipschitz; that is,

$$\left\|\Phi(x_1) - \Phi(x_2)\right\| \le \xi \left\|x_1 - x_2\right\|, \tag{2}$$

where Lipschitz constant $\xi > 0$. Vectors v and w represent Gaussian measurement noise and Gaussian process noise, respectively. And v and w are independent with the following properties:

$$\mathbb{E}[w(t)] = 0, \tag{3a}$$

$$\mathbb{E}\left[w(t_1)w(t_2)^{\mathrm{T}}\right] = Q \cdot \delta(t_1 - t_2), \tag{3b}$$

$$\mathbb{E}[v(k)] = 0, \tag{3c}$$

$$\mathbb{E}\left[v(k_1)v(k_2)^{\mathrm{T}}\right] = R \cdot \delta_{k_1,k_2}, \tag{3d}$$

where $\delta(\cdot)$ is *Dirac delta function* and $\delta_{i,j}$ is *Kronecker delta function*. It should be noted that the continuous-discrete systems like (1a) naturally exist when continuous process are measured via digital sensors. Without loss of generality, we are going to present a nonlinear observer design where the estimation instant is synchronized with the measurements instant since it is exactly what is needed under the background of diagnosis. The proposed CD-FMO will be detailed in the next section.

3. Continuous-Discrete Finite Memory Observer

In this section, the construction of the proposed continuous-discrete finite memory observer for nonlinear systems (1a) is illustrated. Then the finite-time convergence has been proved theoretically. The selection of window length is stated at the end of this section. Before we start, we introduce the following remark first.

Remark 1. The authors in [24] have proven that the observability of a nonlinear dynamic system is a necessary condition and that there exists a finite-time observer for the system.

We are able to conclude from this remark that if we can build a finite-time observer for a nonlinear system, then this nonlinear system is observable.

3.1. Formulation of CD-FMO. Suppose that at each frozen time instant t, the discrete measurements are collected in the most recent time interval $[t - \tau_i, t]$, where $\tau_i = i \times T_s$ and $i = 0, 1, \ldots, L-1$. Here, L is called window length. By using the square matrix exponential e^{-At} as a factor and integrating (1a), we can give the relation between the states in two different time instants t and $t - \tau_i$ as follows:

$$\begin{aligned} x(t) = e^{A\tau_i}x(t-\tau_i) &+ \int_{t-\tau_i}^{t} e^{A(t-\theta)}Bu(\theta)\mathrm{d}\theta \\ &+ \int_{t-\tau_i}^{t} e^{A(t-\theta)}\Phi(x(\theta))\mathrm{d}\theta + \int_{t-\tau_i}^{t} e^{A(t-\theta)}Gw(\theta)\mathrm{d}\theta. \end{aligned} \tag{4}$$

Then, premultiplying (4) by the matrix $Ce^{-A\tau_i}$ and taking into account the measurement equation (1a) at time instant $t - \tau_i$, we obtain

$$Ce^{-A\tau_i}x(t) = y(t-\tau_i) - v(t-\tau_i) + \alpha_{t-\tau_i,t} + \beta_{t-\tau_i,t} + \int_{t-\tau_i}^{t} Ce^{A(t-\tau_i-\theta)}Gw(\theta)\mathrm{d}\theta, \tag{5}$$

with

$$\alpha_{t-\tau_i,t} = \int_{t-\tau_i}^{t} Ce^{A(t-\tau_i-\theta)}Bu(\theta)\mathrm{d}\theta, \tag{6a}$$

$$\beta_{t-\tau_i,t} = \int_{t-\tau_i}^{t} Ce^{A(t-\tau_i-\theta)}\Phi(x(\theta))\mathrm{d}\theta. \tag{6b}$$

Applying (5) for each measurement in the time window $[t-\tau_{L-1}, t]$, a finite number of augmented measurements can be expressed in terms of system state $x(t)$ as in the following linear equation:

$$Y_L - V_L = W_L x(t), \tag{7}$$

where

$$V_L = \begin{pmatrix} v(t-\tau_0) - \int_{t-\tau_0}^{t} Ce^{A(t-\tau_0-\theta)}Gw(\theta)\mathrm{d}\theta \\ v(t-\tau_1) - \int_{t-\tau_1}^{t} Ce^{A(t-\tau_1-\theta)}Gw(\theta)\mathrm{d}\theta \\ \vdots \\ v\left(t-\tau_{L-1} - \int_{t-\tau_{L-1}}^{t} Ce^{A(t-\tau_{L-1}-\theta)}Gw(\theta)\mathrm{d}\theta\right) \end{pmatrix},$$

$$Y_L = \begin{pmatrix} y(t-\tau_0) + \alpha_{t-\tau_0,t} + \beta_{t-\tau_0,t} \\ y(t-\tau_1) + \alpha_{t-\tau_1,t} + \beta_{t-\tau_1,t} \\ \vdots \\ y(t-\tau_{L-1}) + \alpha_{t-\tau_{L-1},t} + \beta_{t-\tau_{L-1},t} \end{pmatrix},$$

$$W_L = \begin{pmatrix} Ce^{-A\tau_0} \\ Ce^{-A\tau_1} \\ \vdots \\ Ce^{-A\tau_{L-1}} \end{pmatrix}. \tag{8}$$

It is straightforward that the noise component V_L has zero mean; that is, $\mathbb{E}(V_L) = 0$. The variance matrix P is block symmetric matrix in the following form:

$$P = \begin{pmatrix} Q_0 & Q_1 & \cdots & Q_{L-1} \\ Q_1 & Q_1 & \cdots & Q_{L-1} \\ \vdots & \vdots & \ddots & \vdots \\ Q_{L-1} & Q_{L-1} & \cdots & Q_{L-1} \end{pmatrix} + \begin{pmatrix} R & 0 & \cdots & 0 \\ 0 & R & \cdots & 0 \\ \vdots & \vdots & \ddots & \vdots \\ 0 & 0 & \cdots & R \end{pmatrix}. \tag{9}$$

where the block elements Q_i with $(i = 0, 1, \ldots, L-1)$ are calculated by

$$Q_i = \int_{-\tau_i}^{0} Ce^{As}GQG^{\mathrm{T}}e^{A^{\mathrm{T}}s}C^{\mathrm{T}}\mathrm{d}s. \tag{10}$$

Now, the state estimation $\widehat{x}(t)$ at time instant t, that is, the solution of (7), can be obtained as follows in the sense of least squares:

$$\widehat{x}(t) = \left(W_L^{\mathrm{T}}P^{-1}W_L\right)^{-1}W_L^{\mathrm{T}}P^{-1}\widehat{Y}_L, \tag{11}$$

with

$$\widehat{Y}_L = \begin{pmatrix} y(t-\tau_0) + \alpha_{t-\tau_0,t} + \widehat{\beta}_{t-\tau_0,t} \\ y(t-\tau_1) + \alpha_{t-\tau_1,t} + \widehat{\beta}_{t-\tau_1,t} \\ \vdots \\ y(t-\tau_{L-1}) + \alpha_{t-\tau_{L-1},t} + \widehat{\beta}_{t-\tau_{L-1},t} \end{pmatrix}, \tag{12a}$$

$$\widehat{\beta}_{t-\tau_i,t} = \int_{t-\tau_i}^{t} Ce^{A(t-\tau_i-\theta)}\Phi(\widehat{x}(\theta))\mathrm{d}\theta. \tag{12b}$$

Let $\Lambda_L = W_L^{\mathrm{T}}P^{-1}W_L$, and it can be seen that the existence condition of $\widehat{x}(t)$ in (11) is given by the existence of matrix Λ_L^{-1}. This condition is then given by the rank of matrix W_L; that is, $\mathrm{rank}(W_L) = n = \dim(x)$, which is guaranteed by the following hypothesis.

Hypothesis 1 (H1). The pair (A, C) is observable.

According to (11) and (12a), we obtain the analytical form of state estimation $\widehat{x}(t)$ for considered nonlinear systems (1a). The calculation of two integral terms $\alpha_{t-\tau_i,t}$ and $\widehat{\beta}_{t-\tau_i,t}$ in (12a) is then detailed as follows.

3.1.1. Analytical Calculation of the Term $\alpha_{t-\tau_i,t}$. It is obvious to see from (6a) that all the elements contained inside the integral are known and it is easy to have an analytical solution by some useful software with symbolic computation such as Maple and Mathematica. If the mathematical expression of input $u(t)$ is unknown, we can still get the solution by putting the element $u(t)$ as a factor of integral under the assumption that $u(t)$ is sampled as zero-order hold and thus remains to be constant between two consecutive sampling instants, which is usually true since most controllers of actual systems are digital computers in practice.

3.1.2. Iterative Algorithm for Solving the Term $\widehat{\beta}_{t-\tau_i,t}$. In order to compute $\widehat{\beta}_{t-\tau_i,t}$, we might also note that it is impossible to have an exact analytical solution. Since we can explicitly see from (12b) that there is the term "$\Phi(\widehat{x}(\theta))$" in the integral, in order to analytically calculate $\widehat{\beta}_{t-\tau_i,t}$, we must know the exact trajectory of "$\widehat{x}(\theta)$" between instant $t-\tau_i$ and t, which unfortunately is what we seek to know (via the estimation $\widehat{x}(t)$ in (11)). Hence, in this paper, a one-step prediction together with iterative-update algorithm is designed to obtain the approximate solution of $\widehat{\beta}_{t-\tau_i,t}$ by Newton-Cotes formulas [25].

In each time window $[t-\tau_{L-1}, t]$, we define the measurement set $Z_L = \{y(t-\tau_i)\}(i = 0, 1, \ldots, L-1)$ and estimation set $\widehat{X}_L = \{\widehat{x}(t-\tau_j)\}(j = 1, \ldots, L-1)$. It should be noted here that there is no case $j = 0$ since all the elements in $\widehat{X}_L$ are obtained by previous window and $\widehat{x}(t-\tau_0) = \widehat{x}(t)$ is exactly what we aim to estimate by current window. Therefore, a one-step prediction of state x at instant t, noted

as $\widehat{x}^*(t)$, has been performed by using the tangent slope $\dot{\widehat{x}}(t-\Delta t)$ with a small time interval $\Delta t = T_s$ as follows:

$$\begin{aligned}\widehat{x}^*(t) &= \widehat{x}(t-\Delta t) + \dot{\widehat{x}}(t-\Delta t)\Delta t \\ &= \widehat{x}(t-T_s) + \dot{\widehat{x}}(t-T_s)T_s \\ &= \widehat{x}(t-\tau_1) + [A\widehat{x}(t-\tau_1) + Bu(t-\tau_1) + \Phi(\widehat{x}(t-\tau_1))]T_s.\end{aligned} \tag{13}$$

$\widehat{x}^*(t)$ is then iteratively updated by (11) and (12a), which makes the finial estimation $\widehat{x}(t)$ after all iterations. The termination condition of the iteration here is given in (14), which is either a threshold γ defined *a priori* for the error between two iterations or a threshold $N_{\max}$ for the number of iterations m:

$$\widehat{x}(t) - \widehat{x}^*(t) \le \gamma \text{ or } m \ge N_{\max}. \tag{14}$$

Furthermore, the first-order Newton-Cotes formula, which yields *trapezoidal rule*, is employed in this paper to numerically approximate the integral term $\widehat{\beta}_{t-\tau_i,t}$ in (12a). For the purpose of reducing the massive computing burden in each iteration, we notice from (12b) that $\widehat{\beta}_{t-\tau_i,t}$ can be divided as follows:

$$\widehat{\beta}_{t-\tau_i,t} = \widehat{\beta}_{t-\tau_i,t-\tau_1} + \widehat{\beta}_{t-\tau_1,t}, \tag{15}$$

with

$$\widehat{\beta}_{t-\tau_i,t-\tau_1} = \int_{t-\tau_i}^{t-\tau_1} Ce^{A(t-\tau_i-\theta)}\Phi(\widehat{x}(\theta))\mathrm{d}\theta, \tag{16a}$$

$$\widehat{\beta}_{t-\tau_1,t} = \int_{t-\tau_1}^{t} Ce^{A(t-\tau_1-\theta)}\Phi(\widehat{x}(\theta))\mathrm{d}\theta, \tag{16b}$$

Let

$$g(\widehat{x}(\theta)) = Ce^{A(t-\tau_i-\theta)}\Phi(\widehat{x}(\theta)), \tag{17}$$

and we know that the previous estimation set $\{\widehat{x}(t-\tau_j)\}$ $(j = 1, \ldots, L-1)$ is unchanged during each iteration of updating $\widehat{x}^*(t)$, which leads to $g(\widehat{x}(t-\tau_j))$ by (17) unchanged. As a consequence, $\widehat{\beta}_{t-\tau_i,t-\tau_1}$ by (16a) also remains the same at each iteration. Therefore, as it is shown in Figure 1, we only need to recalculate the term $\widehat{\beta}_{t-\tau_1,t}$ in (15) at each iteration. In this way, the unnecessary calculation burden caused by iteration can be dramatically reduced when using Newton-Cotes formulas to calculate the numerical integration.

For the sake of overall understanding, the summarized algorithm of the proposed nonlinear observer CD-FMO is shown in Algorithm 1.

3.2. Estimation Property of the Presented CD-FMO

Theorem 1. *If nonlinear system (1a) satisfies the hypothesis H1, in the case of noise-free and fault-free, the property of estimation by presented CD-FMO are unbiased as follows:*

$$\widehat{x}(t) = x(t), \quad t \in [L \times T_s, +\infty). \tag{18}$$

Proof. In the case of noise-free and fault-free, according to (1)–(7), the proposed CD-FMO (11) can be rewritten for the deterministic case as follows:

$$\begin{aligned}\widehat{x}(t) &= \left(W_L^{\mathrm{T}}W_L\right)^{-1}W_L^{\mathrm{T}}\widehat{Y}_L \\ &= \Omega_L^{-1}\sum_{i=0}^{L-1} e^{-A^{\mathrm{T}}\tau_i}C^{\mathrm{T}}\left(y(t-\tau_i) + \alpha_{t-\tau_i,t} + \widehat{\beta}_{t-\tau_i,t}\right),\end{aligned} \tag{19}$$

with

$$\Omega_L = W_L^{\mathrm{T}}W_L = \sum_{i=0}^{L-1} e^{-A^{\mathrm{T}}\tau_i}C^{\mathrm{T}}Ce^{-A\tau_i}, \tag{20}$$

and then, as stated in (5) and regardless of noise term $v(t-\tau_i)$, $y(t-\tau_i)$ can be given as

$$y(t-\tau_i) = Ce^{-A\tau_i}x(t) - \alpha_{t-\tau_i,t} - \beta_{t-\tau_i,t}, \tag{21}$$

and by replacing the term $y(t-\tau_i)$ in (19) by (21) and taking into account (20), we have

$$\begin{aligned}\widehat{x}(t) &= \Omega_L^{-1}\sum_{i=0}^{L-1} e^{-A^{\mathrm{T}}\tau_i}C^{\mathrm{T}}\left(Ce^{-A\tau_i}x(t) - \beta_{t-\tau_i,t} + \widehat{\beta}_{t-\tau_i,t}\right) \\ &= \Omega_L^{-1}\sum_{i=0}^{L-1} e^{-A^{\mathrm{T}}\tau_i}C^{\mathrm{T}}Ce^{-A\tau_i}x(t) + \Omega_L^{-1}\sum_{i=0}^{L-1} e^{-A^{\mathrm{T}}\tau_i}C^{\mathrm{T}} \\ &\quad \cdot \left(\widehat{\beta}_{t-\tau_i,t} - \beta_{t-\tau_i,t}\right) \\ &= x(t) + \Omega_L^{-1}\sum_{i=0}^{L-1} e^{-A^{\mathrm{T}}\tau_i}C^{\mathrm{T}}\left(\widehat{\beta}_{t-\tau_i,t} - \beta_{t-\tau_i,t}\right).\end{aligned} \tag{22}$$

In order to prove Theorem 1, we know that the following equivalence can be obtained directly:

$$\widehat{x}(t) = x(t) \Longleftrightarrow \|\widehat{x}(t) - x(t)\| = 0, \quad t \in [L \times T_s, +\infty), \tag{23}$$

and from (22), together with the properties of matrix norm [26], the norm of $\widehat{x}(t) - x(t)$ can be therefore expressed as follows:

$$\begin{aligned}\|\widehat{x}(t) - x(t)\| &= \left\|\Omega_L^{-1}\sum_{i=0}^{L-1} e^{-A^{\mathrm{T}}\tau_i}C^{\mathrm{T}}\left(\widehat{\beta}_{t-\tau_i,t} - \beta_{t-\tau_i,t}\right)\right\| \\ &\le \sum_{i=0}^{L-1}\left\|\Omega_L^{-1}e^{-A^{\mathrm{T}}\tau_i}C^{\mathrm{T}}\left(\widehat{\beta}_{t-\tau_i,t} - \beta_{t-\tau_i,t}\right)\right\|.\end{aligned} \tag{24}$$

According to (6b) and (12b) and hypothesis **H1**, (24) can be further derived as

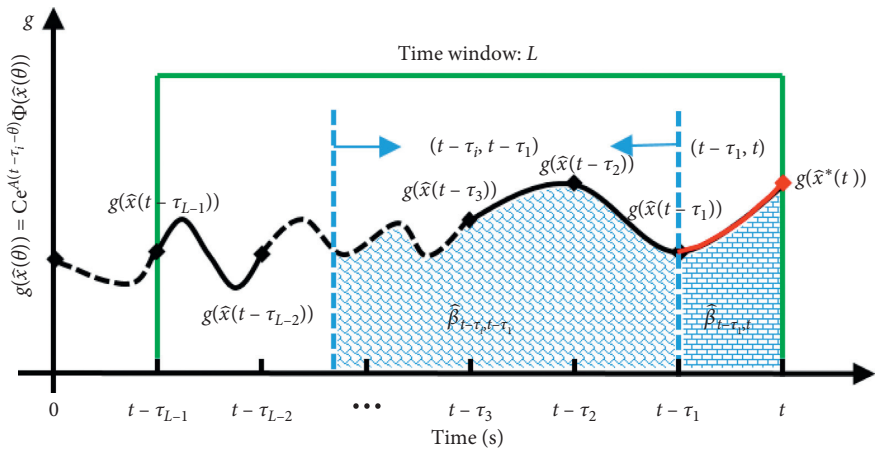

Figure 1: Calculation framework of $\widehat{\beta}_{t-\tau_i,t}$ in each interval $[t-\tau_i, t]$.

Step 1: Initialization ($m = 0$). At each frozen time instant t, given the measurement set Z_L and the previous estimation $\widehat{X}_L$.
Step 2: Calculating $g(\hat{x}(t-\tau_j))$ for all the elements in set $\widehat{X}_L$, then using Newton-Cotes formulas to compute $\widehat{\beta}_{t-\tau_i,t-\tau_1}$ by (16a)
Step 3: Perform a one-step prediction of x at instant t, noted as $\hat{x}^*(t)$, by using $\hat{x}(t-\tau_1)$ and (13).
Step 4: Iterative updating ($m = 1, 2, \ldots, N_{\max}$)
(4a) Calculating $g(\hat{x}^*(t))$ by (17) with the $\hat{x}^*(t)$ predicted in **Step 3**;
(4b) Using Newton-Cotes formulas to obtain $\widehat{\beta}_{t-\tau_1,t}$ by (16b);
(4c) Computing the whole integral term $\widehat{\beta}_{t-\tau_i,t}$ by (15);
(4d) Updating $\hat{x}^*(t)$ as $\hat{x}(t)$ via (11) and (12a);
(4e) *If* $\hat{x}(t) - \hat{x}^*(t) \le \gamma$ or $m \ge N_{\max}$, then terminate iteration; *else* set $m = m + 1$, $\hat{x}^*(t) = \hat{x}(t)$, and go back to **(4a).**
Step 5: Moving the time window to next time instant $t = t + T_s$, and go back to **Step 1.**

Algorithm 1: The summarized nonlinear CD-FMO algorithm.

$$\begin{aligned}
\|\hat{x}(t) - x(t)\| &\le \sum_{i=0}^{L-1} \left\| \Omega_L^{-1} e^{-A^{\mathrm{T}}\tau_i} C^{\mathrm{T}} \int_{t-\tau_i}^{t} Ce^{A(t-\tau_i-\theta)} [\Phi(\hat{x}(\theta)) - \Phi(x(\theta))] \right\| \mathrm{d}\theta \\
&\le \sum_{i=0}^{L-1} \int_{t-\tau_i}^{t} \left\| \Omega_L^{-1} e^{-A^{\mathrm{T}}\tau_i} C^{\mathrm{T}} Ce^{A(t-\tau_i-\theta)} [\Phi(\hat{x}(\theta)) - \Phi(x(\theta))] \right\| \mathrm{d}\theta \\
&\le L \int_{t-\tau_{L-1}}^{t} \left\| \Omega_L^{-1} e^{-A^{\mathrm{T}}\tau_{L-1}} C^{\mathrm{T}} Ce^{A(t-\tau_{L-1}-\theta)} [\Phi(\hat{x}(\theta)) - \Phi(x(\theta))] \right\| \mathrm{d}\theta \\
&\le L \int_{t-\tau_{L-1}}^{t} \left\| \Omega_L^{-1} e^{-A^{\mathrm{T}}\tau_{L-1}} C^{\mathrm{T}} Ce^{A(t-\tau_{L-1}-\theta)} \right\| \|\Phi(\hat{x}(\theta)) - \Phi(x(\theta))\| \mathrm{d}\theta \\
&\le L \int_{t-\tau_{L-1}}^{t} \left\| \Omega_L^{-1} e^{-A^{\mathrm{T}}\tau_{L-1}} C^{\mathrm{T}} Ce^{A(t-\tau_{L-1}-\theta)} \right\| \xi \|\hat{x}(\theta) - x(\theta)\| \mathrm{d}\theta \\
&\le L \int_{L\times T_s}^{t} \left\| \Omega_L^{-1} e^{-A^{\mathrm{T}}\tau_{L-1}} C^{\mathrm{T}} Ce^{A(t-\tau_{L-1}-\theta)} \right\| \xi \|\hat{x}(\theta) - x(\theta)\| \mathrm{d}\theta \\
&= \mathbf{0} + L \int_{L\times T_s}^{t} \left\| \Omega_L^{-1} e^{-A^{\mathrm{T}}\tau_{L-1}} C^{\mathrm{T}} Ce^{A(t-\tau_{L-1}-\theta)} \right\| \xi \|\hat{x}(\theta) - x(\theta)\| \mathrm{d}\theta,
\end{aligned} \tag{25}$$

and then the Gronwall inequality [27] yields

$$\|\hat{x}(t) - x(t)\| \le \mathbf{0} \cdot e^{\int_{L\times T_s}^{t} L \left\| \Omega_L^{-1} e^{-A^{\mathrm{T}}\tau_{L-1}} C^{\mathrm{T}} Ce^{A(t-\tau_{L-1}-\theta)} \right\| \xi \mathrm{d}\theta} = 0, \tag{26}$$

and hence,

$$\|\hat{x}(t) - x(t)\| \le 0 \Longrightarrow \|\hat{x}(t) - x(t)\| = 0 \Longrightarrow \hat{x}(t) = x(t). \tag{27}$$

The proof is completed. □

Remark 2. We can see from Theorem 1 that $\widehat{x}(t) = x(t)$ is always true when $t \geq L \times T_s$; that is to say, we have the following conclusion:

(1) The proposed CD-FMO is a dead-beat observer in the case of noise-free and fault-free; the finite-time convergence is $L \times T_s$ (one window-size).

(2) There is no estimation when $t < L \times T_s$. In other words, there is no initial value problem (IVP) for the presented nonlinear observer, which gives us another advantage for application in physics or other sciences.

3.3. Analytical Choice of the Window Length L. As it is shown in (11) and (12a), at each time instant t, the state estimation $\widehat{x}(t)$ is related to the window length L. Thus, it is necessary to interpret how to select an appropriate window length L. Here, we are going to explain this by defining the "minimal length $L_{\min}$" and "maximal length $L_{\max}$", as it has been shown in [18].

3.3.1. Minimal Length L_{min}. The minimal window length $L_{\min}$ is chosen to assure the existence of the proposed CD-FMO by (11). As we have already discussed in subsection A of Section 3, this condition is then given by the rank of matrix W_L; that is, $\operatorname{rank}(W_L) = n = \dim(x)$, which is already guaranteed by hypothesis H1. However, $L_{\min}$ is just used to valid the hypothesis H1; it is definitely not the optimal window length, as shown in the latter section.

3.3.2. Maximal Length L_{max}. Here it should be noticed that, theoretically speaking, there is no maximum window length $L_{\max}$ for CD-FMO. The greater the length L, the better the estimation $\widehat{x}(t)$, which is reasonable since the amount of measurement information augments as the window length increases. However, after a certain size, the contribution of additional information by increasing window length is not significant enough to decrease estimation error. Therefore, in this paper, we take "the maximum eigenvalue of covariance matrix $\Sigma_{\widetilde{x}}$" of estimation error $\widetilde{x} = \widehat{x} - x$ as an indicator to select maximum window length $L_{\max}$. Given a selected threshold of estimation error tolerance Υ_{Tol}, $L_{\max}$ is defined as follows:

$$L_{\max} = \underset{L}{\operatorname{argmin}}\left\{\max\left(\operatorname{eig}\left(\Sigma_{\widetilde{x}}\right)\right) \leq \Upsilon_{\text{Tol}}\right\}, \tag{28}$$

which is the smallest window length when the largest eigenvalue of $\Sigma_{\widetilde{x}}$ is smaller than error tolerance threshold Υ_{Tol}. This part will be further analyzed in the next section with an illustrative example.

4. Illustrative Example: A Single-Link Robot

In this section, we consider a nonlinear single-link robotic arm, which has an elastic joint rotating in a vertical plane [28]. The nonlinear state-space model is described here as

$$\begin{aligned} \dot{x}(t) &= Ax(t) + Bu(t) + \Phi(x) + Gw(t), \\ y(k) &= Cx(k) + v(k), \end{aligned} \tag{29}$$

with $x = [x_1 \quad x_2 \quad x_3 \quad x_4]^{\mathrm{T}}$. Here, components x_1 and x_3 are the displacement of link and rotor, respectively, while components x_2 and x_4 represent the velocity. The measurement noise $v \sim \mathcal{N}(\mathbf{0}, R)$ and the process noise $w(t) = 0$. The input control $u(t) = 2\sin(2t)$, which is the torque provided by the motor. All the other related matrices are given as follows:

$$\begin{aligned} A &= \begin{pmatrix} 0 & 1 & 0 & 0 \\ -\frac{k}{J_l} & -\frac{F_l}{J_l} & \frac{k}{J_l} & 0 \\ 0 & 0 & 0 & 1 \\ \frac{k}{J_m} & 0 & -\frac{k}{J_m} & -\frac{F_m}{J_m} \end{pmatrix}, \\ B &= \begin{pmatrix} 0 \\ 0 \\ 0 \\ \frac{1}{J_m} \end{pmatrix}, \\ \Phi(x) &= \begin{pmatrix} 0 \\ -\frac{mgl}{J_l}\sin x_1 \\ 0 \\ 0 \end{pmatrix}, \\ C &= \begin{pmatrix} 1 & 0 & 0 & 0 \\ 0 & 0 & 1 & 0 \\ 0 & 0 & 0 & 1 \end{pmatrix}, \\ R &= \begin{pmatrix} 4 \times 10^{-4} & 0 & 0 \\ 0 & 4 \times 10^{-4} & 0 \\ 0 & 0 & 9 \times 10^{-4} \end{pmatrix}. \end{aligned} \tag{30}$$

The simulation scenario is performed according to the following parameters: elastic constant $k = 2$; viscous friction coefficient $F_m = 1$, $F_l = 0.5$; link mass $m = 4$; the rotor inertia of motor $J_m = 1$ and the link inertia $J_l = 2$; mass center $l = 0.5$; $g = 9.8$ is gravity constant. The sampling period

$T_s = 0.01s$. The Lipschitz constant of the considered system is $\xi = 9.8$. The initial conditions for the robotic arm system is

$$x(0) = (1 \quad 1 \quad 1 \quad 1)^{\mathrm{T}}. \tag{31}$$

4.1. Selection of Window Length L. As shown in (28), we take "$\max(\mathrm{eig}(\Sigma_{\tilde{x}}))$" as an indicator to select $L_{\max}$. It can be seen from Figure 2 that the maximum eigenvalue of $\Sigma_{\tilde{x}}$ is asymptotically convergent as window length L increases, which indicates that the estimation performance provided by the presented CD-FMO well improves while the window length augments. After window length $L_1 = 13$, the decrease of the curve is much less significant, which is normal since few additional information can be provided by increasing the window length. This is also why the proposed observer is called "*finite memory*." Nevertheless, starting from $L_2 = 20$, the curve shows a slight trend of going up, which is a normal phenomenon because the approximation error of Newton-Cotes formulas (used in (12a) for integral term $\widehat{\beta}_{t-\tau_i,t}$) will also get bigger as L increases. In order to get a better diagnosis performance, we choose $L = 15$ for all the analysis and diagnosis later in this paper, which is well between L_1 and L_2.

4.2. Numerical Integration Approximation Error Analysis. In order to perform state estimate via (11), we choose *trapezoidal rule* to approximate the integral term $\widehat{\beta}_{t-\tau_i,t}$ in (12a), so it is necessary to give the approximation error bound. We recall the following lemma.

Lemma 1. *Given a definite integral $I = \int_a^b f(x)dx$, the approximation error of trapezoidal rule is [25]*

$$\mathcal{O}(I) = -\frac{(b-a)^3}{12} f''(\eta), \quad \eta \in [a,b]. \tag{32}$$

We can have the following expression of $\hat{x}(t)$ by rewriting (11) as follows:

$$\begin{aligned}\hat{x}(t) &= \left(W_L^{\mathrm{T}} P^{-1} W_L\right)^{-1} W_L^{\mathrm{T}} P^{-1} \hat{Y}_L \\ &= \Lambda_L^{-1} \sum_{i=0}^{L-1} e^{-A^{\mathrm{T}}\tau_i} C^{\mathrm{T}} R^{-1} \left(y(t-\tau_i) + \alpha_{t-\tau_i,t} + \widehat{\beta}_{t-\tau_i,t}\right),\end{aligned} \tag{33}$$

and together with (12b) and (17), we extract the integral term related to $\widehat{\beta}_{t-\tau_i,t}$ and noted as

$$\mathcal{B}_{t-\tau_i,t} = \Lambda_L^{-1} \sum_{i=0}^{L-1} e^{-A^{\mathrm{T}}\tau_i} C^{\mathrm{T}} R^{-1} \left(\int_{t-\tau_i}^{t} g(\hat{x}(\theta)) \mathrm{d}\theta \right), \tag{34}$$

and we can see from $\mathcal{B}_{t-\tau_i,t}$ that the calculation of approximation error by using trapezoidal rule can be divided into two steps:

(i) **Step** 1: Calculate the upper approximation error bound $|\mathcal{O}(Int)|$ with $Int = \int_{t-T_s}^{t} g(\hat{x}(\theta))\mathrm{d}\theta$

(ii) **Step** 2: Calculate cumulative error bound Γ_{nc} as i varies in the summation $\sum_{i=0}^{L-1}$

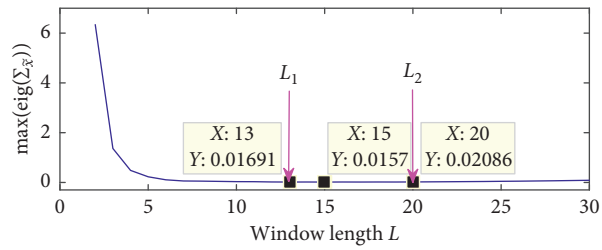

Figure 2: Convergence of covariance $\Sigma_{\tilde{x}}$ with window length L increases.

For Step 1, according to Lemma 1, the bound of approximation error $\mathcal{O}(Int)$ can be described as follows:

$$|\mathcal{O}(Int)| \le \frac{T_s^3}{12} \max_{\theta \in [t-T_s,t]} \left| g''(\hat{x}(\theta)) \right|. \tag{35}$$

And from expression (17), we can get the first and second derivatives of g as follows:

$$\begin{aligned} g'(\hat{x}(\theta)) &= \frac{\mathrm{d}g(\hat{x}(\theta))}{\mathrm{d}\theta} = -Ce^{A(t-\tau_i-\theta)} A\Phi(\hat{x}(\theta)) \\ &\quad + Ce^{A(t-\tau_i-\theta)} \frac{\mathrm{d}\Phi(\hat{x}(\theta))}{\mathrm{d}\hat{x}} \frac{\mathrm{d}\hat{x}(\theta)}{\mathrm{d}\theta}, \\ g''(\hat{x}(\theta)) &= \frac{\mathrm{d}^2 g(\hat{x}(\theta))}{\mathrm{d}\theta^2} = \frac{\mathrm{d}g'(\hat{x}(\theta))}{\mathrm{d}\theta} \\ &= Ce^{A(t-\tau_i-\theta)} A^2 \Phi(\hat{x}(\theta)) - 2Ce^{A(t-\tau_i-\theta)} A \\ &\quad \cdot \frac{\mathrm{d}\Phi(\hat{x}(\theta))}{\mathrm{d}\hat{x}} \frac{\mathrm{d}\hat{x}(\theta)}{\mathrm{d}\theta} + Ce^{A(t-\tau_i-\theta)} \frac{\mathrm{d}}{\mathrm{d}\theta} \\ &\quad \cdot \left(\frac{\mathrm{d}\Phi(\hat{x}(\theta))}{\mathrm{d}\hat{x}} \frac{\mathrm{d}\hat{x}(\theta)}{\mathrm{d}\theta} \right), \end{aligned} \tag{36}$$

and we omit the details of how to calculate each item in g'' in this paper. By calculating the norm of g'' together with the parameters defined at the beginning of this section, we have

$$|\mathcal{O}(Int)| \le 2.5228 \times 10^{-6} \triangleq \zeta_{t-T_s,t}. \tag{37}$$

For Step 2, we can directly get the cumulative error bound Γ_{nc} as i varies in the summation $\sum_{i=0}^{L-1}$ as follows:

$$\begin{aligned} \Gamma_{nc} &\le 0 + \zeta_{t-T_s,t} + 2\zeta_{t-T_s,t} + \cdots + (L-1)\zeta_{t-T_s,t} \\ &= \frac{L(L-1)}{2} \zeta_{t-T_s,t} \\ &= 2.6489 \times 10^{-4}, \quad (L = 15), \end{aligned} \tag{38}$$

and meanwhile, the maximum element of standard deviation (SD) σ of measurement noise, noted as $\sigma_{\max}$, is given by

$$\sigma\sigma^{\mathrm{T}} = R \Rightarrow \sigma = R^{1/2} = \begin{pmatrix} 2\times10^{-2} & 0 & 0 \\ 0 & 2\times10^{-2} & 0 \\ 0 & 0 & 3\times10^{-2} \end{pmatrix} \Longrightarrow \sigma_{\max} = 3\times10^{-2}. \tag{39}$$

It is obvious that $\Gamma_{nc} \ll \sigma_{\max}$, which means that the approximation error for numerical integration is drowned in measurement noise. As a result, we can conclude that our estimation is correct with window length $L = 15$.

4.3. State Estimation Performance. It can be clearly seen from Figure 3 that four-dimensional system state x is reconstructed correctly under the presence of measurement noise and the proposed CD-FMO provides great performance of state estimation. Besides, Figure 3 also depicts how the accuracy of state estimation gets much better as window length L gets longer, which is another consistent result with respect to Figure 2.

4.3.1. Unbiased Estimation Property Analysis in Stochastic Case. As has been proved in Theorem 1 for the deterministic case, the unbiased estimation property of presented nonlinear observer under the presence of measurement noise,

$$\mathbb{E}(\widehat{x}(t) - x(t)) = 0, \quad \text{or } (\mathbb{E}(\widehat{x}(t)) = x(t)), \tag{40}$$

is evaluated by root-mean-square error (RMSE) criteria together with Monte Carlo (MC) simulation, where RMSE is defined as $\mathrm{RMSE} = \sqrt{(1/N_{\mathrm{mc}})\sum_{i=1}^{N_{\mathrm{mc}}}(\widehat{x}^{(i)} - x)^2}$ and N_{mc} represents MC simulation times. The state estimation by running multiple MC simulation is therefore defined in the average sense: $\widehat{x}_{\mathrm{mean}} = (1/N_{\mathrm{mc}})\sum_{i=1}^{N_{\mathrm{mc}}}\widehat{x}^{(i)}$.

Let N_{mc} take the values 100 and 500, respectively. By taking the component x_1 as an example, it can be seen from Figure 4 that, during the MC simulations, the estimation upper and lower bounds of $\widehat{x}$ are quiet small, which means that the state estimation by proposed CD-FMO varies within a small range around real state x in the presence of measurement noise. Moreover, the estimation $\widehat{x}_{\mathrm{mean}}$ obtained by $N_{\mathrm{mc}} = 500$ is closer to true value than the one by $N_{\mathrm{mc}} = 100$, which is logical since MC simulation performed a series of repeated random sampling of Gaussian measurement noise; the larger the sampling size is, the closer the mean value of noise is to zero.

The unbiased estimation property has also been examined by the RMSE with different N_{mc} in Figure 5. We can see that the RMSEs are close to zero; meanwhile, the RMSE of $N_{\mathrm{mc}} = 500$ is smoother than the one $N_{\mathrm{mc}} = 100$. This means that the results obtained by two criteria are consistent.

To summarize what has been mentioned above, we have established by Monte Carlo simulation that state estimation given by the presented nonlinear observer CD-FMO in the stochastic case is also unbiased; that is, $\mathbb{E}(\widehat{x}(t) - x(t)) = 0$. This property provides a good precondition for the fault diagnosis after-step.

4.3.2. Robustness Analysis with respect to Measurement Noise. We are going to analyze the robustness of CD-FMO against measurement noise through three scenarios shown in Table 1. Measurement noise varies from σ to 0.5σ and 1.5σ ($\pm 50\%$), respectively, while the parameter setting of observer does not change, which means that the proposed observer (11) has an inconsistency between $y(\cdot)$ in (12a) and noise parameter P for observer.

By taking x_1 as an example, it can be seen from Figure 6(a) that the state estimations $\widehat{x}_1$ can still well follow the trajectory of true state x_1 even if the measurement noise has $\pm 50\%$ variations, which shows the robustness of CD-FMO vis-a-vis measurement noise. In addition, we can see from the RMSEs in Figure 6(b) that state estimation of Scenario 1 is better than Scenario 2. It is logical because of the following reason: we have chosen $L = 15$ for the considered robotic arm system. In fact, CD-FMO with $L = 15$ in Scenario 2 has already performed a little role of "*filter*" for this nonlinear system. As shown in Figure 2, when $L = 15$, $\max(\mathrm{eig}(\Sigma_{\widetilde{x}})) = 0.0157$, while the minimum noise level in this case (minimum nonzero value of σ) is 0.02; that is, $\sigma_{\min} = 0.02$. The fact of $\max(\mathrm{eig}(\Sigma_{\widetilde{x}})) \leq \sigma_{\min}$ means that the largest dispersion of estimation is still smaller than the minimum noise level, which is the performance of a filter. Accordingly, when we use the same window length for an even lower noise level, that is, Scenario 1, the presented CD-FMO will still perform as a filter and maybe even more. That is why we get a better estimation even when CD-FMO "overestimate" the real noise level.

5. Application to Fault Diagnosis

In this section, we are going to apply the proposed CD-FMO to perform the fault diagnosis of the considered nonlinear single-link robotic arm system. In order to deal with all faults in the same simulation launch, we suppose that each fault only occurs during certain period $[T_{\mathrm{fs}}, T_{\mathrm{fe}}]$; therefore, we use the following function to characterize the fault duration:

$$\Pi(t, T_{\mathrm{fs}}, T_{\mathrm{fe}}) = H(t - T_{\mathrm{fs}}) - H(t - T_{\mathrm{fe}}), \tag{41}$$

where $H(\cdot)$ is *Heaviside step function*. In this paper, we injected two kinds of typical faults as follows:

(1) Sensor bias*:* a sudden bias is one of the abrupt sensor faults, which is modeled as

$$y_{\mathrm{f}} = y + \Pi(t, T_{\mathrm{fs}}, T_{\mathrm{fe}})I\Delta. \tag{42}$$

A bias on y_1 (**F1**): $I = I_{y_1} = [1 \quad 0 \quad 0]^{\mathrm{T}}$, $\Delta = \Delta_{y_1} = 0.15$, fault period $[T_{\mathrm{fs}}, T_{\mathrm{fe}}] = [0.5\,\mathrm{s}, 1.0\,\mathrm{s}]$.

A bias on y_2 (**F2**): $I = I_{y_2} = [0 \quad 1 \quad 0]^{\mathrm{T}}$, $\Delta = \Delta_{y_2} = 0.15$, fault period $[T_{\mathrm{fs}}, T_{\mathrm{fe}}] = [2.0\,\mathrm{s}, 2.5\,\mathrm{s}]$.

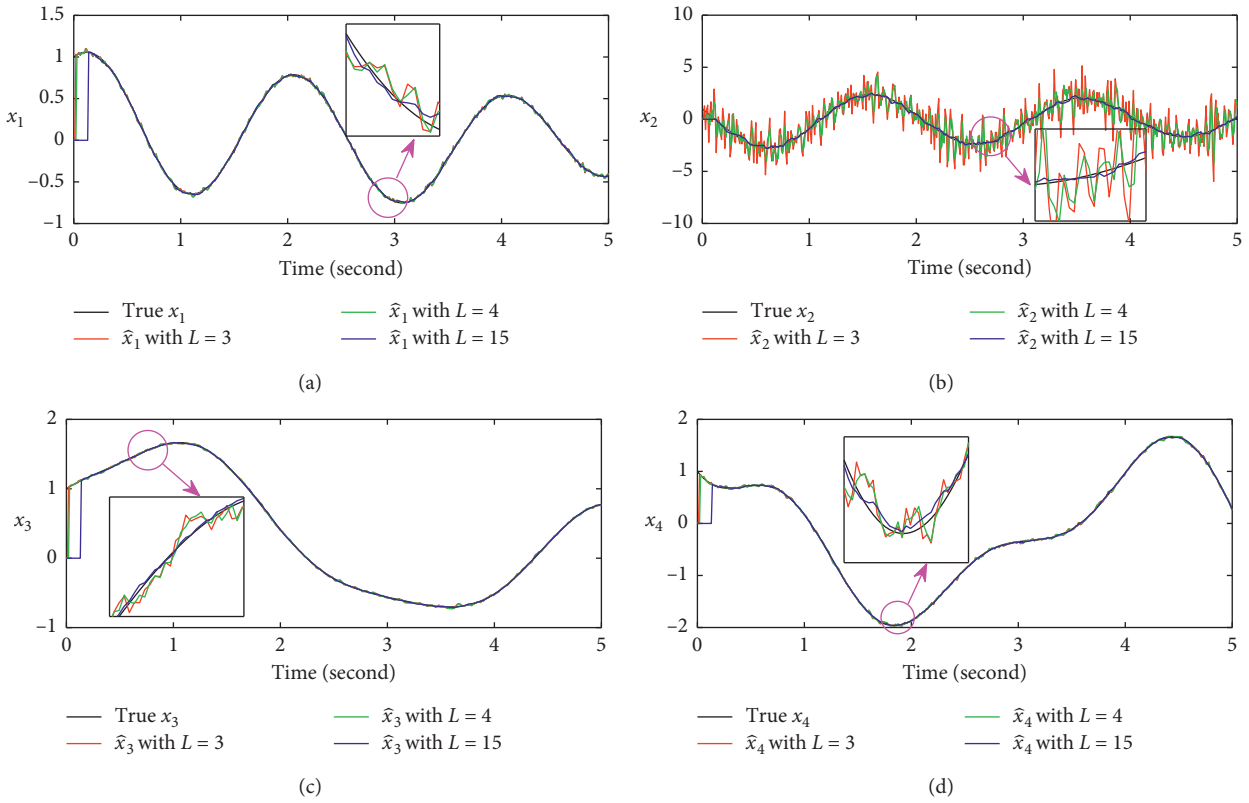

FIGURE 3: State estimation $\hat{x}$ with different window lengths L. (a) Estimation of x_1. (b) Estimation of x_2. (c) Estimation of x_3. (d) Estimation of x_4.

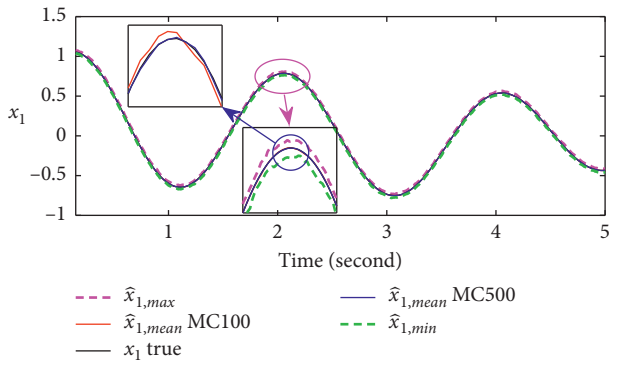

FIGURE 4: Upper (lower) bound and mean of $\hat{x}_1$ between $N_{mc} = 100$ and $N_{mc} = 500$.

A bias on y_3 (**F3**): $I = I_{y_3} = [0 \quad 0 \quad 1]^T$, $\Delta = \Delta_{y_3} = -0.15$, fault period $[T_{fs}, T_{fe}] = [3.5\,\text{s}, 4.0\,\text{s}]$.

(2) Actuator fault: we modelize the actuator fault as

$$u_f = \Pi(t, T_{fs}, T_{fe})(1 - \rho)u, \tag{43}$$

where $\rho \in [0, 1]$ *describes* control loss level. $\rho = 0$ means there is no actuator fault, whereas $\rho = 1$ signifies that the control is completely lost.

Actuator fault (**F4**): $\rho = 0.6$, $[T_{fs}, T_{fe}] = [5.0\,\text{s}, 5.5\,\text{s}]$.

5.1. Fault Detection. In this paper, *residuals* are chosen as fault indicators, and it is defined as follows:

$$r(t) = y(t) - C\hat{x}(t), \tag{44}$$

with $t = k \times T_s$, which checks the consistency of real measurements of system and measurements estimated by the proposed CD-FMO. We use both residual r and the Cumulative Sum (CUSUM) control charts of r for the reason that CUSUM control chart is well-known as the efficiency of detecting small change in the mean of a sequence. As introduced in [29], the upper CUSUM $G^+(k)$ and lower CUSUM $G^-(k)$ of residuals sequences $r(k)$ (with mean μ_r and SD σ_r) are defined as follows:

$$\begin{cases} G^+(k) = \max\{0, G^+(k-1) + r(k) - \mu_r - K\}, \\ G^-(k) = \min\{0, G^-(k-1) + r(k) - \mu_r + K\}, \end{cases} \tag{45}$$

with the starting value $G^+(0) = G^-(0) = 0$. The detection criterion is as follows:

$$G^+(k) > H \text{ or } G^-(k) < -H, \tag{46}$$

and in order to quickly detect the small shift in mean, the parameters of CUSUM control chart is set as $K = (1/2)\sigma_r$ and $H = 3\sigma_r$.

In the presence of measurement noise, CUSUM control chart can improve the performance of diagnosis. For example, in Figure 7(a), the change of residual r_1 is not very obvious during fault **F3** occurs, but it can be clearly seen from the CUSUM chart of r_1 in Figure 7(b). CUSUM chart can also help

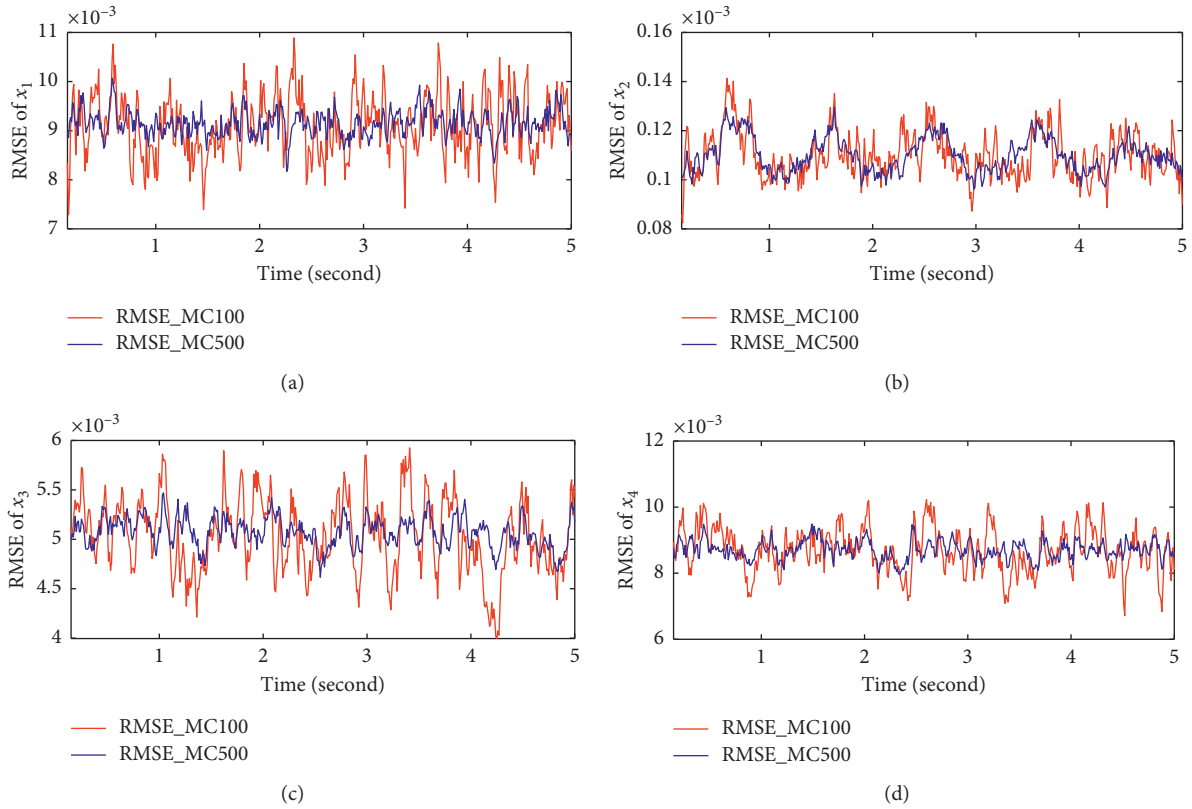

Figure 5: RMSE comparison between $N_{\text{mc}} = 100$ and $N_{\text{mc}} = 500$.

Table 1: Different scenarios of SD for measurement noise.

Measurement noise scenarios settings		CD-FMO parameter settings
Scenario 1	SD = 0.5σ	$R = \sigma^2$
Scenario 2	SD = σ	$P = \text{diag}(R, R, \ldots, R)$
Scenario 3	SD = 1.5σ	

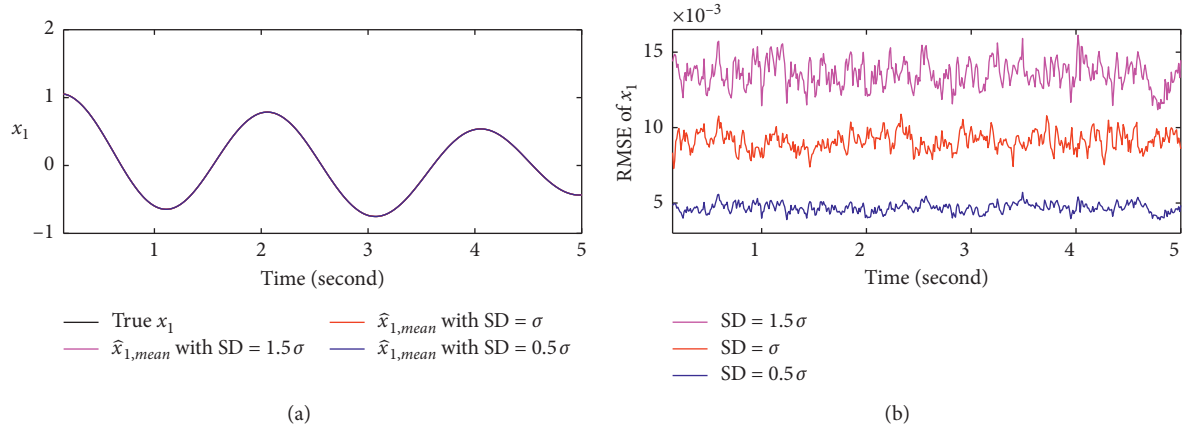

Figure 6: Robustness analysis in different measurement noise scenarios. (a) Estimation of x_1 in different measurement noise scenarios. (b) RMSE in different measurement noise scenarios.

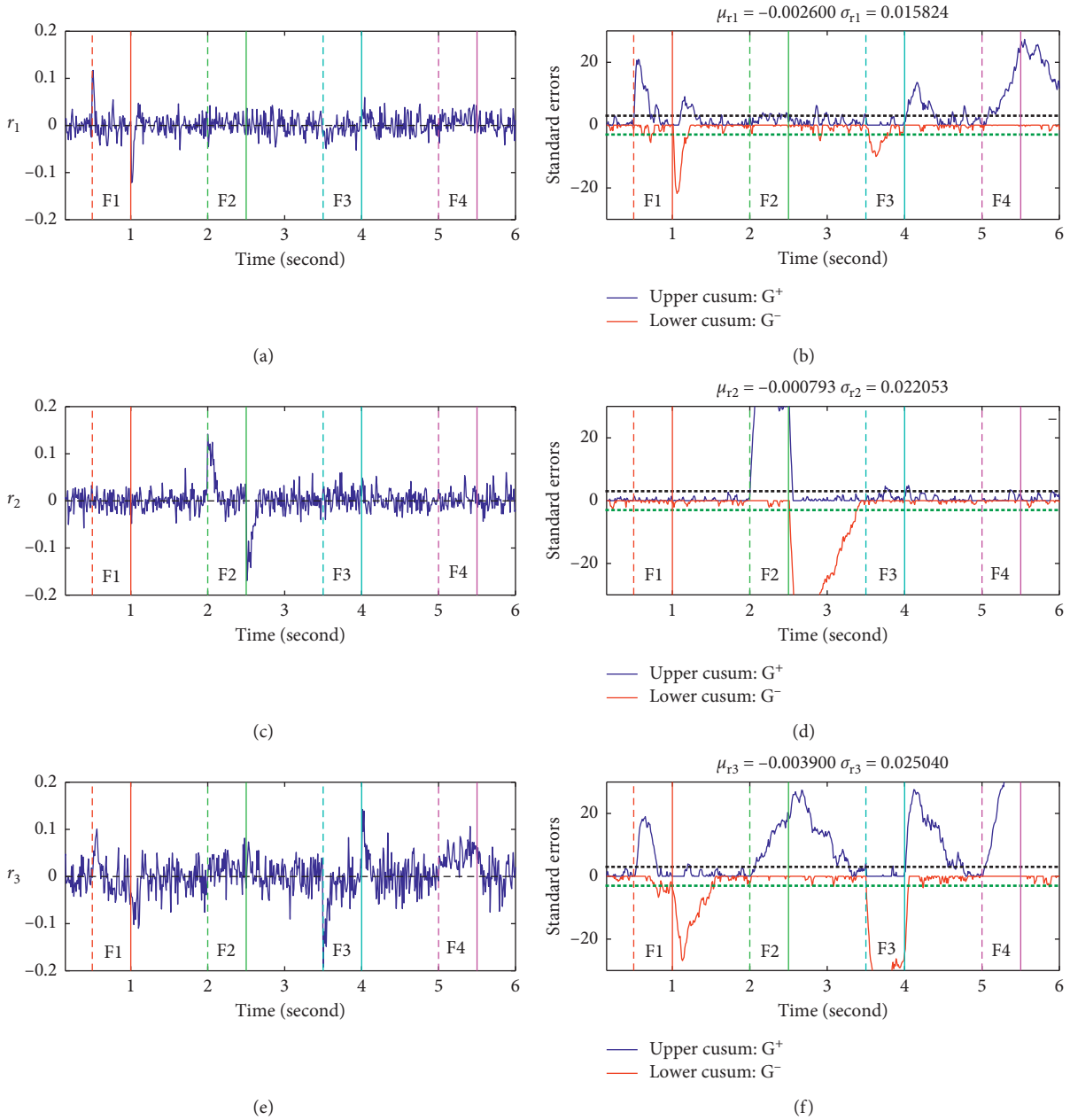

FIGURE 7: Residual r and the CUSUM control chart of r. (a) Residual r_1. (b) CUSUM control chart of residual r_1. (c) Residual r_2. (d) CUSUM control chart of residual r_2. (e) Residual r_3. (f) CUSUM control chart of residual r_3.

to detect the incipient fault such as **F4** more quickly, as shown in Figures 7(a) and 7(b). Fault signature of residual r and fault detection instant T_d with respect to different faults are therefore given in Table 2. These results reveal that the proposed CD-FMO has a good and effective performance in both sensor and actuator fault detection for the single-link robotic arm.

5.2. Fault Isolation. It can be obviously seen from Table 2 that fault **F2** is isolable as it has a unique fault signature $[0, 1, 1]$. On the other hand, the remaining three faults **F1**, **F3**, and **F4** cannot be isolated because of the identical fault signature $[1, 0, 1]$. Hence, in this subsection, we aim to solve this problem by using generalized observer scheme (GOS) [30] with another additional observer (CD-FMO 2), while CD-FMO 1 is the same as the previous part. The structure of a bank of CD-FMO is illustrated in Figure 8(a). In this paper, CD-FMO 2 is constructed by choosing subset measurements y_1 and y_3; then the corresponding model parameter changes from C to C_{13}, where C_{13} is composed by the first and third rows of C. Here, state estimation provided by CD-FMO 2 is noted as $\hat{x}'$; therefore, the residual in this case is

$$r'(t) = y(t) - C\hat{x}'(t). \tag{47}$$

The results of r' are shown in Figures 8(b)–8(d), respectively. It shows that all the faults can be detected by residual r_2', while **F1** and **F3** are also detected by r_1' and r_3'.

Table 2: Fault signature for different faults.

Different faults	Start instant T_{fs} (vertical dash line)	End instant T_{fe} (vertical solid line)	Signature			Detect instant T_d
			r_1	r_2	r_3	
A bias on y_1 (**F1**)	0.5 s	1.0 s	1	0	1	0.5 s
A bias on y_2 (**F2**)	2.0 s	2.5 s	0	1	1	2.0 s
A bias on y_3 (**F3**)	3.5 s	4.0 s	1	0	1	3.5 s
Actuator fault (**F4**)	5.0 s	5.5 s	1	0	1	5.05 s

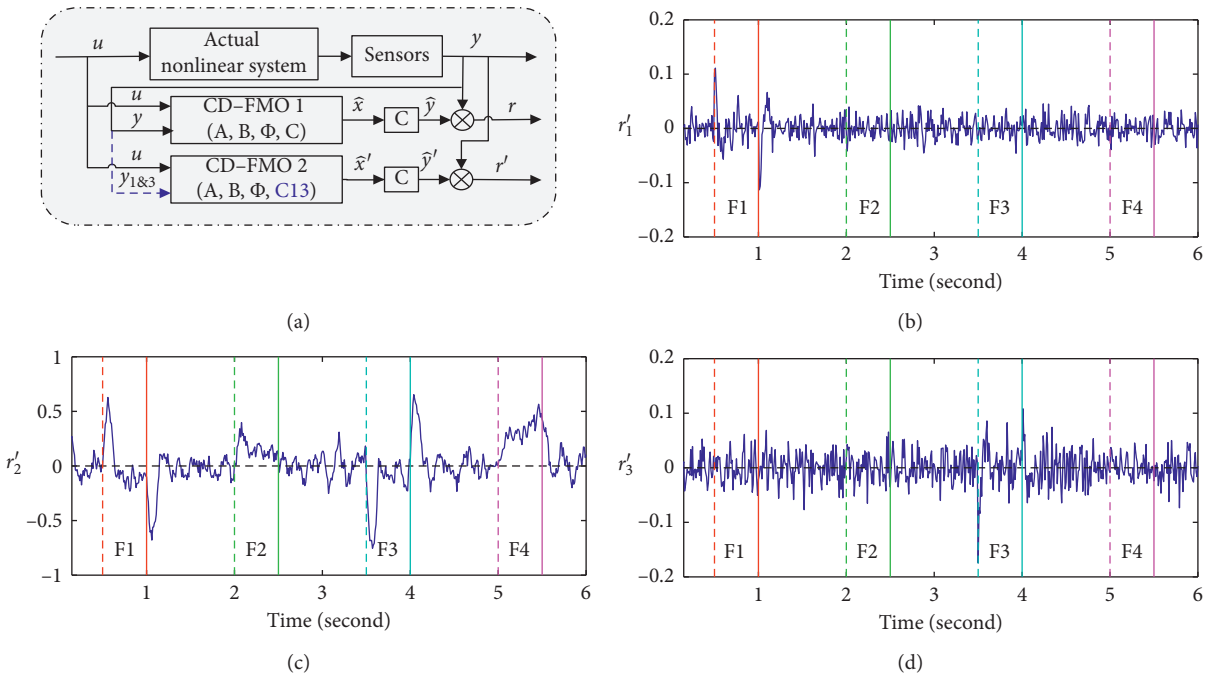

Figure 8: GOS of CD-FMOs and residual $r\prime$ of CD-FMO 2. (a) The scheme for a bank of CD-FMO. (b) Residual r_1' of CD-FMO 2. (c) Residual r_2' of CD-FMO 2. (d) Residual r_3' of CD-FMO 2.

Table 3: Fault signature by CD-FMO 1 and CD-FMO 2.

Different faults	Fault signature CD-FMO 1			Fault signature CD-FMO 2		
	r_1	r_2	r_3	r_1'	r_2'	r_3'
A bias on y_1 (**F1**)	1	0	1	1	1	0
A bias on y_2 (**F2**)	0	1	1	0	1	0
A bias on y_3 (**F3**)	1	0	1	0	1	1
Actuator fault (**F4**)	1	0	1	0	1	0

By comparing the fault signature obtained by CD-FMO 1 and CD-FMO 2 in Table 3, we can obviously see that the three indistinguishable faults **F1**, **F3**, and **F4**, which have identical fault signature $[1, 0, 1]$ by CD-FMO 1, become isolable with $[1, 1, 0]$, $[0, 1, 1]$, and $[0, 1, 0]$ by CD-FMO 2. It means that by applying the GOS structure, the presented CD-FMO can also accomplish the objective of fault isolation effectively.

6. Conclusion

In this paper, a nonlinear observer has been proposed to perform state estimation and fault diagnosis for a class of continuous-discrete nonlinear dynamical systems. The performance of state estimation is great and can be significantly improved by choosing a larger window length. Also the presented approach has a finite-time convergence, which is a great advantage from the perspective of FDI. Simulations have illustrated that the proposed method provides a quite effective fault detection for sensor and actuator faults, which can also show the robustness of this nonlinear observer against the measurement noise. Meanwhile, by using the bank of observers, we are able to deal with the isolation of faults with identical fault signature. It is worth noting that the proposed observer structure can also be apply to the following cases: (1) estimation instant is not synchronized with measurement instant; that is, we are able to obtain the state estimation $\widehat{x}(t)$ with $t \in (kT_s, (k+1)T_s)$. (2) The sampling period of measurement is not a constant;

that is, $T_s \neq constant$. One perspective of the presented CD-FMO is to take the modeling uncertainties into consideration, which are the usual disturbances in practical engineering systems. The other perspective is to give a theoretical sensitivity analysis for different types of faults, which might give more decision-making basis for fault detection as the first step of fault diagnosis.

Data Availability

The code used to support the findings of this study is available from the corresponding author upon request.

Conflicts of Interest

The authors declare that there are no conflicts of interest regarding the publication of this paper.

Acknowledgments

The authors would like to gratefully acknowledge the financial support of the China Scholarship Council (CSC) via the project UT-INSA.

References

[1] P. M. Frank, "Fault diagnosis in dynamic systems using analytical and knowledge-based redundancy," *Automatica*, vol. 26, no. 3, pp. 459–474, 1990.

[2] T. E. Dy Liacco, "The role and implementation of state estimation in an energy management system," *International Journal of Electrical Power & Energy Systems*, vol. 12, no. 2, pp. 75–79, 1990.

[3] S. A. Ali, A. Christen, S. Begg, and N. Langlois, "Continuous-discrete time-observer design for state and disturbance estimation of electro-hydraulic actuator systems," *IEEE Transactions on Industrial Electronics*, vol. 63, no. 7, pp. 4314–4324, 2016.

[4] A. J. Krener and I. Alberto, "Linearization by output injection and nonlinear observers," *Systems & Control Letters*, vol. 3, no. 1, pp. 47–52, 1983.

[5] D. Bestle and M. Zeitz, "Canonical form observer design for non-linear time-variable systems," *International Journal of Control*, vol. 38, no. 2, pp. 419–431, 1983.

[6] G. Phanomchoeng and R. Rajamani, "Observer design for Lipschitz nonlinear systems using Riccati equations," in *Proceedings of the 2010 American Control Conference*, pp. 6060–6065, Baltimore, MD, USA, 2010.

[7] C. Huang and H. Huang, "Observer-based robust preview tracking control for a class of non-linear systems," *IET Control Theory & Applications*, vol. 14, no. 7, pp. 991–998, 2020.

[8] T. N. Dinh, V. Andrieu, M. Nadri, and U. Serres, "Continuous-discrete time observer design for Lipschitz systems with sampled measurements," *IEEE Transactions on Automatic Control*, vol. 60, no. 3, pp. 787–792, 2015.

[9] J. Huang, L. Yu, and M. Shi, "Observer design for stochastic one-sided Lipschitz Lur'e differential inclusion system," *International Journal of Computer Mathematics*, vol. 97, no. 3, pp. 624–637, 2020.

[10] A. H. Jazwinski, *Stochastic Processes and Filtering Theory*, Dover, New York, NY, USA, 2013.

[11] C. Ling and C. Kravaris, "Multirate sampled-data observer design based on a continuous-time design," *IEEE Transactions on Automatic Control*, vol. 64, no. 12, pp. 5265–5272, 2019.

[12] M. Farza and M. M'Saad, "Busawon K\enleadertwodots continuous-discrete-time observers for a class of uniformly observable systems," in *Hybrid Dynamical Systems. Lecture Notes in Control and Information Sciences*, M. Djemai and M. Defoort, Eds., Vol. 457, Springer, Berlin, Germany, 2015.

[13] X. Han, Z. Li, B. Dahhou, M. Cabassud, and M. He, "Nonlinear observer based fault diagnosis for an innovative intensified heat-exchanger/reactor," in *Proceedings of the 11th International Conference on Modelling, Identification and Control (ICMIC2019)*, vol. 582, Springer, Singapore, 2020.

[14] Z. Bougatef, N. Abdelkrim, A. Aitouche, and M. N. Abdelkrim, "Fault detection of a PEMFC system based on delayed LPV observer," *International Journal of Hydrogen Energy*, vol. 45, no. 19, pp. 11233–11241, 2020.

[15] L. Li, M. Chadli, S. X. Ding, J. Qiu, and Y. Yang, "Diagnostic observer design for T-S fuzzy systems: application to real-time-weighted fault-detection approach," *IEEE Transactions on Fuzzy Systems*, vol. 26, no. 2, pp. 805–816, 2018.

[16] M. Toda and R. Patel, "Performance bounds for continuous-time filters in the presence of modeling errors," *IEEE Transactions on Aerospace and Electronic Systems*, vol. 14, no. 6, pp. 912–919, 1978.

[17] H. Heffes, "The effect of erroneous models on the Kalman filter response," *IEEE Transactions on Automatic Control*, vol. 11, no. 3, pp. 541–543, 1966.

[18] G. Graton, F. Kratz, and J. Fantini, "Finite Memory Observers for linear time-varying systems: theory and diagnosis applications," *Journal of the Franklin Institute*, vol. 351, no. 2, pp. 785–810, 2014.

[19] H. W. Sorenson and J. E. Sacks, "Recursive fading memory filtering," *Information Sciences*, vol. 3, no. 2, pp. 101–119, 1971.

[20] A. V. Medvedev and H. T. Toivonen, *A Continuous Finite-Memory Deadbeat Observer*, American Control Conference, Chicago, IL, USA, 1992.

[21] W. Nuninger, F. Kratz, and J. Ragot, "Finite memory generalised state observer approach for failure detection in dynamic systems," in *Proceedings 37th IEEE Conference on Decision and Control*, pp. 581–585, Tampa, 1998.

[22] J. Thuillier, D. Delouche, J. Fantini, and F. Kratz, "Finite Memory Observer-based sensor fault detection and isolation for system when measurements are correlated with process noise," *Safeprocess*, vol. 51, no. 24, pp. 320–325, 2018.

[23] R. Kajdan, G. Graton, D. Aubry, and F. Kratz, "fault detection of a nonlinear switching system using finite memory observer," *IFAC Proceedings Volumes*, vol. 39, no. 13, pp. 992–997, 2006.

[24] S. R. Kou, T. Tarn, and D. L. Elliott, "Finite-time observer for nonlinear dynamic systems," in *Proceedings of the IEEE Conference on Decision and Control*, pp. 116–119, San Diego, CA, USA, 1973.

[25] K. E. Atkinson, *An Introduction to Numerical Analysis*pp. 252-253, John Wiley & Sons, New York, NY, USA, 2nd edition, 1989.

[26] C. Mayer, *Matrix Analysis and Applied Linear Algebra Book and Solutions Manuel*, SIAM, Philadelphia, PA, USA, 2001.

[27] R. Bellman, "The stability of solutions of linear differential equations," *Duke Mathematical Journal*, vol. 10, no. 4, pp. 643–647, 1943.

[28] X. Zhang, M. Polycarpou, and T. Parisini, "Design and analysis of a fault isolation scheme for a class of uncertain

nonlinear systems," *Annual Reviews in Control*, vol. 32, no. 1, pp. 107–121, 2008.

[29] D. C. Montgomery, *Introduction to Statistical Quality Control*, Wiley, Hoboken, NJ, USA, 6th edition, 2013.

[30] P. M. Frank, "Fault diagnosis in dynamic systems via state estimation-a survey," in *System Fault Diagnostics, Reliability and Related Knowledge-Based Approaches*, S. Tzafestas, M. Singh, and G. Schmidt, Eds., Springer, Dordrecht, PA, USA, 1987.